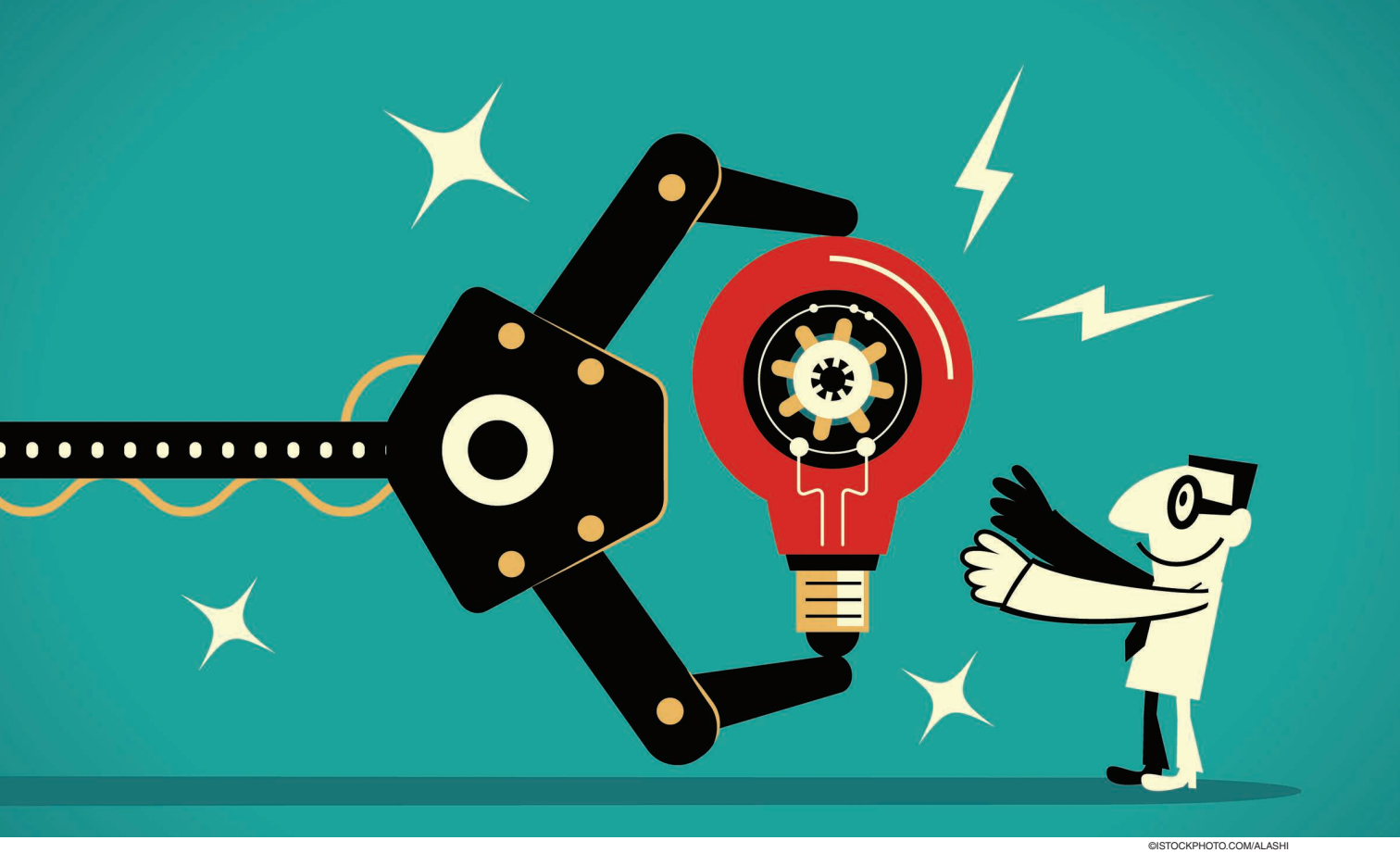

©ISTOCKPHOTO.COM/ALASHI

Adaptable Workstations for Human–Robot Collaboration

A Reconfigurable Framework for Improving Worker Ergonomics and Productivity

By Wansoo Kim, Marta Lorenzini, Pietro Balatti, Phuong D.H. Nguyen, Ugo Pattacini, Vadim Tikhanoff, Luka Peternel, Claudio Fantacci, Lorenzo Natale, Giorgio Metta, and Arash Ajoudani

Digital Object Identifier 10.1109/MRA.2018.2890460
Date of publication: 6 March 2019

Musculoskeletal disorders, the single largest category of work-related injuries in many industrial countries, are associated with very high costs in terms of lost productivity. In high-volume production facilities, large parts of the workstation should ideally be adapted to individual workers in real time to prevent such injuries. However, in smaller production lines, especially those found in small and medium enterprises (SMEs), regularly adapting the entire workstation to accommodate flexibility is a major challenge. A solution to the problem is the development of reconfigurable human–robot collaboration (HRC) workstations and frameworks. These are key to enabling agile manufacturing, by merging the dexterity, flexibility, and

1070-9932/19©2019IEEE

problem-solving ability of humans with the strength and precision of robotics.

In this direction, we propose a novel HRC framework that enables real-time adaptation to human dynamic factors and intentions. The first is associated with the overloading of the body joints, while the latter determines whether or not a certain part is intended to be manipulated, whether the worker is left or right handed, or that the worker has moved within the workspace. Robot responses are then framed to help the worker perform the intended manipulation task in configurations where the effect of external loads on body joints is at a minimum. An experimental evaluation of the proposed framework on 10 subjects is provided to demonstrate the potential for industrial applications.

The Need for an Adaptive HRC Framework

Several industrial duties require forceful, repetitive, or sustained movements that may result in cumulative trauma, increasing the risk for work-related musculoskeletal disorders. In large manufacturing facilities, such duties are usually well defined and have led to the publication of suitable training procedures and workstation design standards to ensure that workers follow ergonomics best practices [1].

The transition of such technologies and procedures to SMEs is more problematic in terms of economic sustainability [2] because of the implementation costs and SMEs' low-volume, high-mix production processes. The latter represent a larger barrier, mainly due to the requirements for customized production, changing prototypes, and so on. Therefore, highly adaptive and quickly reconfigurable systems with real-time data processing capabilities are required to address the ergonomics issues in SMEs while also ensuring productivity.

A potential solution is the development of HRC workstations that combine human dexterity and capacity for problem solving with the precision, endurance, and power of robotics [3], [4]. Nevertheless, collaborative robots (called *cobots*) are rarely thought of as being physically coupled with human coworkers to provide assistance. In fact, most existing real-time HRC frameworks are built around the concept of *human avoidance* to ensure safety, i.e., avoiding accidental collisions between humans and robots carrying sharp or heavy industrial objects. These frameworks follow suitable guidelines published in international standards, such as the International Organization for Standardization's technical specification 15066, to account for the force, pressure, and velocity limits of the cobots given the hardware characteristics [5]. Although this safety aspect is crucial for cobots to work with humans, the controlled use of physical assistance by cobots should not be neglected.

Early works to achieve this aimed to develop HRC frameworks that physically couple humans and robots. Examples of applications include cocarrying [6], [7] and comanipulation [8]–[10], among others. These frameworks usually process the interaction forces induced by human operators and the environment to control robot movements, but they do not take into account human factors and the delivered effort. Other offline processing techniques are available for the inclusion of human factors in HRC systems, with applications oriented toward workstation or cobot mechanical design [11], [12], but these cannot be easily incorporated into industrial applications having fast-reconfigurability demands. In fact, most existing standard techniques used to study human ergonomics are based on offline processing of human kinematic movements and the environment [13]. This approach cannot be considered for realistic collaborative tasks due to the dynamic interactions between humans and the external world (robot and the environment).

To equip cobots with the additional capability of real-time processing of human states while collaborating with humans, our recent work [14] proposed a method to estimate human body joint loadings caused by external forces. The method was built on the displacement of the human whole-body center of pressure (CoP) in the support plane, which was caused by the application of an external force. This consideration reduced the number of subject-specific dynamic model parameters to be identified, compared with previous techniques that required the identification of various model parameters to account for full dynamics [15].

This article extends our previous work in several ways and aims to create a unified ergonomic and reconfigurable HRC framework. To enhance the cost efficiency and applicability of human tracking in industrial workplaces, the wearable sensory suit used in our previous work is replaced by an external, low-cost red-green-blue depth vision system equipped with a real-time multiperson keypoint detection library. The multiperson algorithms detect the human in a 2D image and then reconstruct the 3D body pose by using a disparity map while applying a number of biophysical constraints [16]. The vision system also tracks the movements of the operator in the robot's workspace, the tool [17], and the operating hand (right or left) during the execution of the task (see Figure 1).

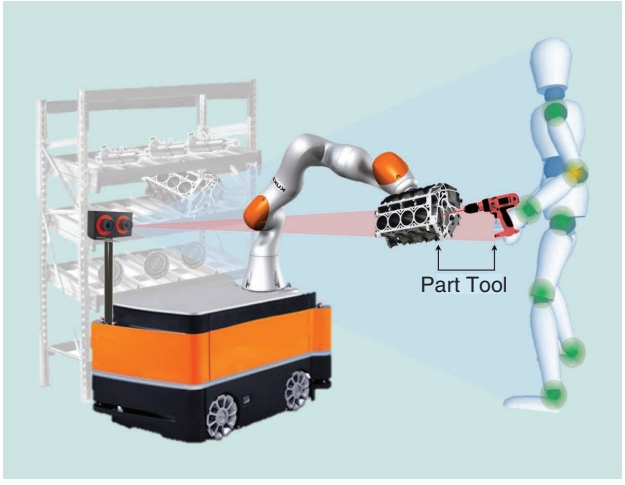

Figure 1. The proposed HRC framework aims to improve worker ergonomics and productivity in competitive manufacturing environments. This is achieved, first, by the real-time perception of human kinematic and dynamic states, tools, and the environment. On this basis, appropriate robot responses are framed to enable adaptability to task variations and human factors.

The human kinematic data together with the tool properties are used to estimate the human body overloading torques, those variations of body joint torques caused by an external load. The algorithm is based on [18] and calculates the center of mass (CoM) of a human with and without the detected tool. From this point, the overloading values of joint torques are estimated online and used by the robot optimization process to guide the human coworker toward an ergonomic configuration to perform the task. In this pose, the effect of tool load on body joints is minimal. A visual feedback interface is developed to guide the operator toward the optimized configurations. Furthermore, to follow the operator's preferred locations within the robot workspace, the vision system tracks human movements; consequently, the robot trajectories are regulated to achieve the task.

A visual feedback interface is developed to guide the operator toward the optimized configurations.

In industrial production/assembly lines, the processes are usually known, and each task (for example, drilling, screwing, polishing, and so on) is associated with a certain tool–part combination (see Figure 2). Hence, improved adaptability of the cobot to human intentions can be achieved by an online detection of the tool. The robot has a reactive response so that a target part is automatically detected and provided to the operator for manipulation. For instance, if a user picks a polisher or a drill, the robot detects the specific tool and grasps and picks the correct part associated with the tool, providing it to the operator while ensuring the best use of the individual's physical capabilities.

In summary, the proposed HRC framework enables robot adaptation to human kinematic and dynamic states and to task variations. To our knowledge, this is the first attempt to integrate several human-centered mechatronics and software components to grant a certain level of autonomy in achieving adaptive and ergonomic HRC. The fast reconfiguration of the proposed HRC framework for new users and production processes can be achieved simply by including new user model parameters and tool–part combinations, highlighting the time and cost efficiency of the proposed technique. In the following, we provide details of the individual components of this framework and present experimental results on 10 healthy subjects of different ages and genders to evaluate the actual performance of the system.

The HRC Framework

The proposed HRC framework is composed of several parts: human whole-body pose tracking, tool recognition, estimation of joint torque overloading, robot interaction and optimization control, and the graphical interface. Here, we describe in more detail the implementation of each of the components and their integration to form a unified HRC framework.

Human Whole-Body Kinematic Tracking

Human whole-body kinematic tracking provides kinematic body configurations extracted directly from the stereovision cameras' input images (monochrome in this case). The algorithm extends the work proposed by Nguyen et al. [16], which originally consisted of two successive phases. In the first phase, the 2D poses of the main human keypoints (that is, head, shoulders, elbows, hands, hips, knees, and ankles) are detected within the images of a stereovision system. Unlike [16], we adopt here the OpenPose deep-learning model [19] pretrained on the COCO (for Common Objects in Context) data set [20], with the goal of identifying and tracking all workers visible in the scene while guaranteeing a sufficient level of accuracy. The outcome of this phase is a set of pixels [*ui*, *vi*] representing the keypoints of all workers' bodies.

In the second phase, we estimate the 3D coordinates of each keypoint pixel $[u_i, v_i]$ (with respect to the camera frame) by projecting it and its $(N-1)$ neighbors through the disparity map from standard stereo geometry:

$$x_i = \frac{1}{N}\sum_{k}^{N}\frac{(u_i^k - w/2)\cdot t}{d^k},$$
$$y_i = \frac{1}{N}\sum_{k}^{N}\frac{(v_i^k - h/2)\cdot t}{d^k},$$
$$z_i = \frac{1}{N}\sum_{k}^{N}\frac{f\cdot t}{d^k}, \quad (1)$$

where w and h are the image dimensions, t is the stereo baseline, d^k is the disparity value at pixel $[u_i^k, v_i^k]$ (the kth neighbor pixel of the keypoint pixel $[u_i, v_i]$), and f is the focal length after rectification. In this setting, N is empirically set to eight, which gives us the best estimation results.

Subsequently, on the basis of the 3D knowledge acquired in the previous

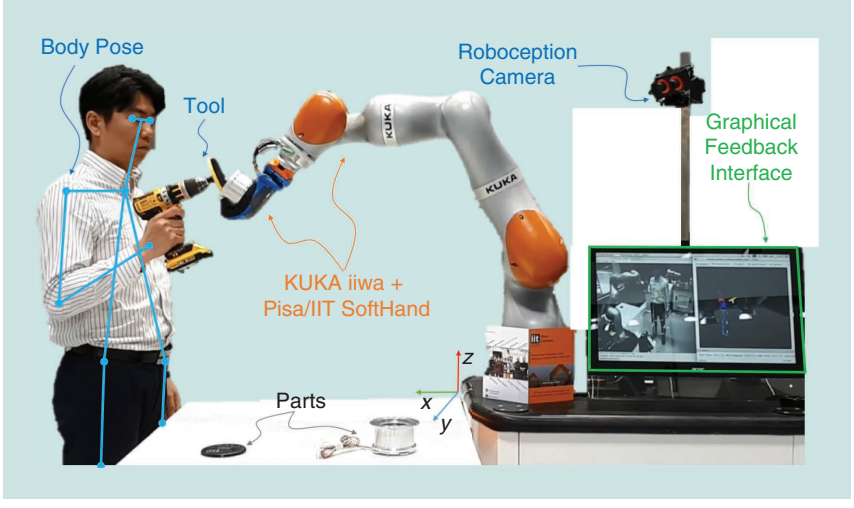

Figure 2. The HRC experimental setup in this study.

step and the workspace bounds known in advance, we can filter out the workers belonging to the background and obtain only the partner who is actively collaborating with the robot. (This was a crucial requirement for the KUKA Innovation Award because several visitors were expected to be close to the scene and visible to the camera.) Finally, to further refine the set of 3D keypoints, we use median filtering with a window size of 11 samples for all keypoints independently; we also apply biophysical constraints, such as admissible ranges of human body dimensions (to avoid undersized or oversized body parts). Therefore, a limb that does not comply with the biophysical bounds because of occlusions or wrong projections of the keypoints is automatically adjusted such that its size is normalized within the allowed range, while its pose in the 3D space is retained. It should be noticed that in our HRC framework, the Roboception [33] camera (shown in Figure 2) produces monochrome images at a rate of 25 Hz, while the disparity map is computed onboard and streamed at 18 Hz.

Tool Recognition

To allow the robot to recognize the tool held by the human partner, we adopt the object teaching and recognition methodology proposed by Pasquale et al. [17]. The detection of the partner's hands in the scene is solved by recruiting the keypoint pixels representing the hands as a result of the 2D pose computation. Thus, with this information, we are able to extract suitable bounding boxes in the images that contain the hands (with or without a tool). The cropped images serve as an input to the downstream image-recognition system composed of a cascade of a CaffeNet [21] deep neural network for features extraction and a regularized least-square linear classifier. The system finally outputs the classification scores computed over all of the object classes with which it has been trained. In this article, we use three classes that correspond to a free hand, a drill, and a polisher (Figure 3).

In certain body configurations, the tool was not fully visible to the camera. This could potentially introduce errors in recognition. To address this issue, the output of the classifier is further improved by means of a temporal filter that introduces a voting mechanism to cast the score of each class, as observed during a given time window. The tool class that receives the highest score throughout the time window represents the predicted tool.

The whole vision framework, as shown in the vision module of Figure 4, is implemented based on YARP middleware [22], [23] and communicates with the other modules of the HRC framework via User Datagram Protocol (UDP) connections.

Joint Torque Overloading

Central to the development of the ergonomic HRC system is a procedure for estimating the overloading of human joint torques, that is, the loading effect of an external force/object on human joints. The method, which was previously proposed in [14], is built on the displacement of the whole-body CoP in the support plane (xy) under two conditions: the results from body dynamics themselves (inertial, Coriolis, centrifugal, and gravity forces) and exposure to external forces. This calculation of the CoP displacement eliminates body dynamics from the resulting equation, which implies that the number of subject-specific parameters to be identified can be significantly reduced.

An extension to this approach proposed in [18] eliminates the need to use additional sensory systems (for example, force plate and sensor insoles) to measure the CoP and ground reaction force (GRF) when an external load is applied to the human body. The assumption behind this choice is the known properties of the external load: because we target the use of tools for manipulating parts in industrial-use cases, this assumption is valid, but it implies that the tools' mass properties must be previously known and stored. As a result, the human CoP model can be updated to include the additional mass at the operator's hand. It is worth noting here that the detection of the tool and whether it is held by the right or left hand is performed autonomously using the vision

The proposed HRC framework enables robot adaptation to human kinematic and dynamic states and to task variations.

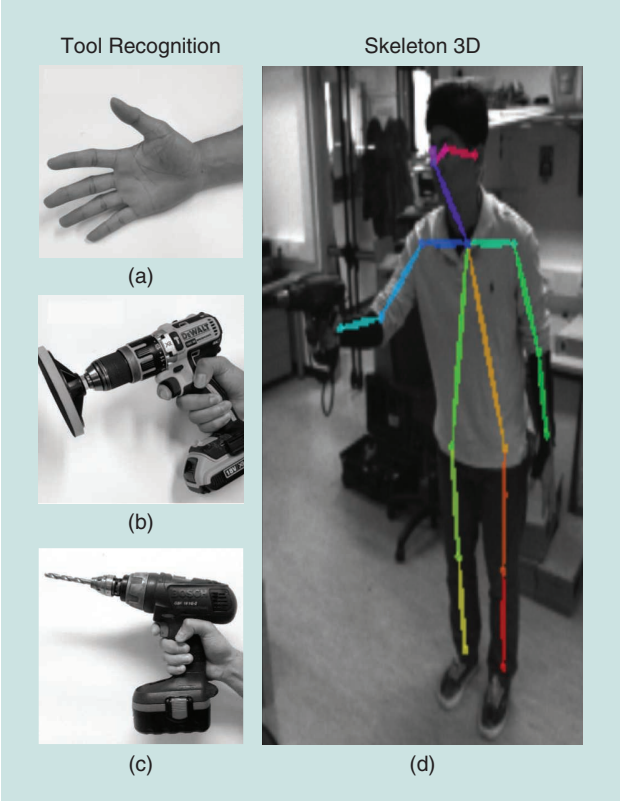

Figure 3. Samples of different classes in the demo: (a) the free hand, (b) polisher, and (c) drill and (d) a snapshot of the human pose estimation result.

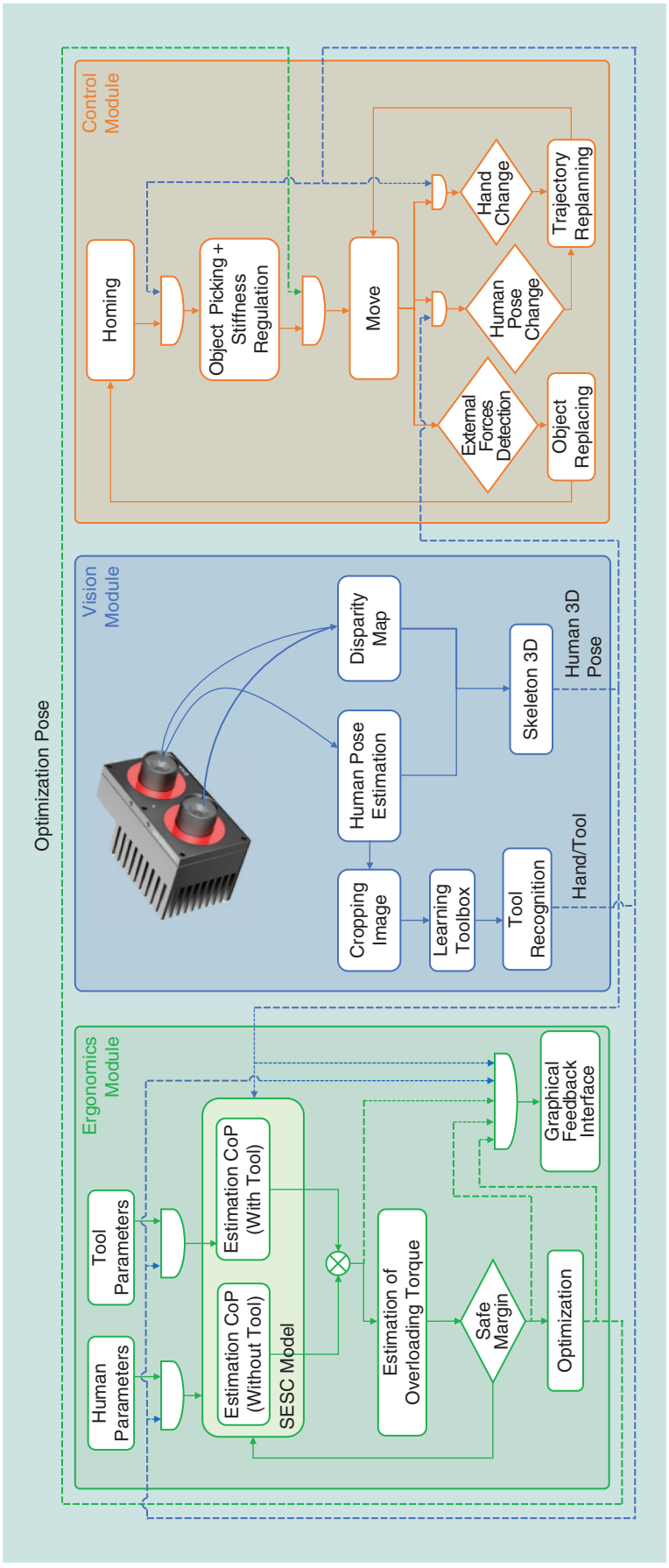

Figure 4. The HRC framework subdivided in three modules (ergonomics, vision, and control). Each module runs in real time and conveys data to the other modules by the User Datagram Protocol (UDP) connection (dotted line). SESC: statically equivalent serial chain.

system. Once the tool type is detected, the mass of the tool can be included in the CoP model.

Next, we provide a brief overview of the algorithm presented in [18]. The human floating base frame Σ_0 was positioned at the pelvis link and connected from the inertial frame Σ_W by a six-virtual degrees of freedom (DoF) chain. We assumed the links were rigid and articulated through n revolute joints, and we defined a local reference frame Σ_i at each joint. The robot base frame Σ_B was defined at the robot's base link. The endpoint of the human was at the human hand frame Σ_H, and the endpoint of the robot was at the robot tool frame Σ_T, both of which were connected to the external objects such as parts (i.e., work pieces).

The joint torque overloading vector can be defined by the relation between the GRF (with and without the effect of an interaction force) and the CoP displacement due to the external load. The relation between n_k contact points and the resultant contact force can be expressed by the Lagrangian equation of motion with respect to Σ_W,

$$\mathbf{M}(\mathbf{q}_h)\ddot{\mathbf{q}}_h + \mathbf{C}(\mathbf{q}_h, \dot{\mathbf{q}}_h)\dot{\mathbf{q}}_h + \mathbf{G}(\mathbf{q}_h) = \mathbf{S}^T\boldsymbol{\tau} + \sum_{i=1}^{n_k} \mathbf{J}^T{}_{p_i}(\mathbf{q}_h)\mathbf{f}_i, \tag{2}$$

where $\mathbf{M}$, $\mathbf{C}$, and $\mathbf{G}$ represent the inertia matrix, the centrifugal and Coriolis forces, and the vector of gravity force, respectively. The generalized coordinates of the system are defined as $\mathbf{q}_h = [\mathbf{x}_0^T \ \boldsymbol{\theta}_0^T \ \mathbf{q}_{h_a}^T]^T \in \mathbb{R}^{6+n}$, where n is the number of DoF in the model. $\mathbf{x}_0 \in \mathbb{R}^3$ and $\boldsymbol{\theta}_0 \in \mathbb{R}^3$ represent the position and orientation of Σ_0 with respect to Σ_W, while $\mathbf{q}_{h_a}$ represents angular positions of human joints. In addition, $\mathbf{S} = [\mathbf{0}_{n\times 6} \ \mathbf{I}_{n\times n}] \in \mathbb{R}^{n\times(n+6)}$ is the actuation matrix, $\boldsymbol{\tau} \in \mathbb{R}^n$ is the vector of applied joint torques, and $\mathbf{J}_{p_i}(\mathbf{q}_h)$ is the contact Jacobian at point $\mathbf{p}_i$, where the contact forces $\mathbf{f}_i$ are applied with respect to Σ_W.

In our approach, we calculate the CoP using the whole-body CoM position and acceleration obtained from the human model. In the static condition, the ground-projected CoM corresponds to the CoP. In the dynamic condition, the difference between the CoP and the projected whole-body CoM highly correlates with the

angular acceleration of the body [24]. Deriving from this, we can obtain the CoP components on the contact surface in the dynamic condition as [25]

$$C_{P\alpha} = C_{M\alpha} - \frac{(C_{Mz} - C_{Pz})}{\ddot{C}_{Mz} + g}\ddot{C}_{M\alpha},\ \alpha = \{x, y\}, \tag{3}$$

where g is the gravitational constant, C_{Px} and C_{Py} are positions of the CoP in the x axis and y axis, C_{Pz} is the height of the ground, and $C_M = [C_{Mx}\ \ C_{My}\ \ C_{Mz}]^T \in \mathbb{R}^3$ is the CoM vector. If the ground is flat and not moving with respect to Σ_W, then C_{Pz} becomes zero. Therefore, we consider only the second derivative of the CoM vector and g to determine the CoP of the human body. To obtain the acceleration of the CoM vector, we use the Kalman filtering approach [26].

For the purposes of this article, the calculation of the whole-body CoM is based on a geometric model presented in [27], known as the *SESC technique*. This model contains a number of subject-specific parameters that must be identified offline. The complete procedure for one-time-only parameter identification is described in [14] and will not be repeated here. Furthermore, to reduce the number of sensory systems for the measurement of the whole-body CoP when an external force is applied (C_{Pw}, required for the calculation of joint torque overloading, as described in the following paragraphs), based on [18], a modified SESC model is developed. This model includes an external object's mass properties, m_e, at the right or left arm endpoint, all of which are detected by the vision system.

To estimate joint torque overloading, we use the difference between the estimated CoP $\hat{C}_{P_{wo}}$ from the human body model without the external object and the CoP $\hat{C}_{P_{wt}}$ from the body model with the external object. The condition without the external object produces a torque vector

$$\mathbf{S}^T\boldsymbol{\tau}_{wo} = \boldsymbol{\tau}_b - \sum_{i=1}^{n_f}\mathbf{J}^T_{\hat{C}_{P_{woi}}}(\mathbf{q}_h)\mathbf{f}_{wo,i}, \tag{4}$$

where $\boldsymbol{\tau}_b = \mathbf{M}(\mathbf{q}_h)\ddot{\mathbf{q}}_\mathbf{h} + \mathbf{C}(\mathbf{q}_h, \dot{\mathbf{q}}_\mathbf{h})\dot{\mathbf{q}}_\mathbf{h} + \mathbf{G}(\mathbf{q}_h) \in \mathbb{R}^{n+6}$ is the joint torque vector of the human body without any external contact (that is, without the ground contact as well) and $\mathbf{f}_{wo}$ is the vertical GRF (vGRF) in this condition, which can be estimated by the human body mass. $n_f \in \{0, \ldots, f \leq 2\}$ is the number of ground contact points at the foot.

On the other hand, the condition with the external object produces a torque

$$\mathbf{S}^T\boldsymbol{\tau}_{wt} = \boldsymbol{\tau}_h - \sum_{i=1}^{n_f}\mathbf{J}^T_{\hat{C}_{P_{wti}}}(\mathbf{q}_h)\mathbf{f}_{wt,i} - \sum_{j=1}^{n_h}\mathbf{J}^T_{a_{hj}}(\mathbf{q}_h)\mathbf{f}_{h,j}, \tag{5}$$

where $\mathbf{f}_{wt}$ is the vGRF, which can be estimated by the combined mass of the human body and the external object. $n_h \in \{0, \ldots, h \leq 2\}$ is the number of contact points where the interaction forces are applied.

The relationship between the interaction force $\mathbf{f}_h$ and vGRF variation $\Delta\mathbf{f}_{w,i} = \mathbf{f}_{wt,i} - \mathbf{f}_{wo,i}$ can be defined as

$$\Delta\mathbf{F} = \sum_{i=1}^{n_f}\Delta\mathbf{f}_{w,i} = -\sum_{j=1}^{n_h}\mathbf{f}_{h,j}. \tag{6}$$

We consider an approximate distribution gain for vGRF and interaction forces $(0 \leq \zeta_i, \eta_j \leq 1)$. Each gain can be distributed according to the body configuration over the number of contact points n_f and n_h, respectively [28], [29]. Deriving from (4)–(6), the overloading joint torque can be defined as

$$\begin{aligned}\Delta\boldsymbol{\tau}_s &= \sum_{j=1}^{n_h}\mathbf{J}^T_{a_{hj}}(\mathbf{q}_h)\eta_j\Delta\mathbf{F} \\ &\quad - \sum_{i=1}^{n_f}\{[\mathbf{J}^T_{\hat{C}_{P_{wti}}}(\mathbf{q}_h) - \mathbf{J}^T_{\hat{C}_{P_{woi}}}(\mathbf{q}_h)]\mathbf{f}_{wt,i} + \mathbf{J}^T_{\hat{C}_{Pi}}(\mathbf{q}_h)\zeta_i\Delta\mathbf{F}\}.\end{aligned} \tag{7}$$

It is important to note that $\boldsymbol{\tau}_b$ does not affect the overloading joint torque vector $\Delta\boldsymbol{\tau}_s$ in any configuration.

Robot Interaction Controller

To achieve safe and adaptive physical interactions between humans and cobots, robot hardware with torque control (or similar) capacity and a lightweight structure is desirable. In this way, one can plan for robot interactions at the end effector to perform the primary task and achieve a suitable null-space behavior to execute lower-hierarchy tasks, e.g., safely treating accidental collisions. Hence, our setup used a KUKA LBR iiwa robot, the vector of whose joint torques $\boldsymbol{\tau} \in \mathbb{R}^7$ is calculated by [30]

$$\boldsymbol{\tau}_r = \mathbf{M}(\mathbf{q}_r)\ddot{\mathbf{q}}_r + \mathbf{C}_r(\mathbf{q}_r, \dot{\mathbf{q}}_r)\dot{\mathbf{q}}_r + \mathbf{g}(\mathbf{q}_r) + \boldsymbol{\tau}_{\text{ext}_r}, \tag{8}$$

with $\boldsymbol{\tau}_{\text{ext}_r} = \mathbf{J}_r^T\mathbf{F}_{c_r} + \tau_{st}$, where $\mathbf{q}_r \in \mathbb{R}^7$ is the joint angles vector, $\mathbf{J}_r \in \mathbb{R}^{6\times7}$ is the robot arm Jacobian matrix, $\mathbf{M}_r \in \mathbb{R}^{7\times7}$ is the mass matrix, $\mathbf{C}_r \in \mathbb{R}^{7\times7}$ is the Coriolis and centrifugal matrix, $\mathbf{g}_r \in \mathbb{R}^7$ is the gravity vector, and $\boldsymbol{\tau}_{\text{ext}_r}$ is the external torque vector. $\mathbf{F}_{c_r}$ represents the forces vector in the Cartesian space, and $\boldsymbol{\tau}_{\text{st}}$ are the second task torques projected onto the null space of $\mathbf{J}_r$.

The quasi-static relationship between the environmental displacements and Cartesian forces $\mathbf{F}_{c_r} \in \mathbb{R}^6$ can be governed by the choices of stiffness $\mathbf{K}_c \in \mathbb{R}^{6\times6}$ and damping $\mathbf{D}_c \in \mathbb{R}^{6\times6}$ parameters, by

$$\mathbf{F}_{c_r} = \mathbf{K}_c(\mathbf{X}_d - \mathbf{X}_a) + \mathbf{D}_c(\dot{\mathbf{X}}_d - \dot{\mathbf{X}}_a), \tag{9}$$

where $\mathbf{X}_d$ and $\mathbf{X}_a \in \mathbb{R}^6$ represent the Cartesian desired and actual position, with $\dot{\mathbf{X}}_d$ and $\dot{\mathbf{X}}_d \in \mathbb{R}^6$ being their corresponding velocity profiles, respectively. The Cartesian stiffness, by default, was set to 1,500 N/m in all of the translational and 150 Nm/rad in all of the rotational Cartesian directions to have a reasonable tradeoff between the tracking performance (due to joint friction and other nonmodeled dynamics) and human safety in case of an

accidental collision at the end effector. The null-space stiffness was always set to a low value (100 Nm/rad) using a stiffness-consistent projection [31] so that a collision with a human or the environment can be treated softly. No other considerations were taken into account for redundancy resolution of the KUKA iiwa robot.

The damping matrix was calculated based on the desired stiffness matrix, using the double diagonalization design,

$$\mathbf{D}_c = 2\mathbf{Q}(\mathbf{q}_r)\mathbf{D}_\xi \mathbf{K}_{d0}^{\frac{1}{2}}\mathbf{Q}^T(\mathbf{q}_r), \tag{10}$$

with $\mathbf{K}_c = \mathbf{Q}(\mathbf{q}_r)\mathbf{K}_{d0}\mathbf{Q}^T(\mathbf{q}_r)$ given the diagonal matrix $\mathbf{K}_{d0}$ (see details in [30]). $\mathbf{D}_\xi = \text{diag}\{\xi_i\}$ is also a diagonal matrix, with the damping factor ξ_i set to 0.7 to achieve a critically damped behavior.

We provide details of the individual components of this framework and present experimental results on 10 healthy subjects of different ages and genders to evaluate the actual performance of the system.

To facilitate the operator's movements in achieving ergonomic configurations during comanipulation, the robot trajectories were adaptively modulated depending on three states: the human position in the robot workspace, the operating hand (left or right), and the overloading condition. The robot's Cartesian stiffness and damping parameters were preset and not optimized during the interaction. Through visual detection of the human body pose and operating hand, an ergonomic body configuration was determined by online minimization of overloading of the human joint torques. A symmetric positive, definite weight matrix $\mathbb{W} = \text{diag}[\Delta\boldsymbol{\tau}_1/\boldsymbol{\tau}_{\max_1} \ \cdots \ \Delta\boldsymbol{\tau}_n/\boldsymbol{\tau}_{\max_n}] \in \mathbb{R}^{n\times n}$, with components $\boldsymbol{\tau}_{\max_n}$ chosen from biomechanical data [32], was considered to assign higher priorities to the highly overloaded body joints. Consequently, the optimization process was defined as

$$\min_{\mathbf{q}_h} \ \| \Delta\boldsymbol{\tau}^T \mathbb{W} \Delta\boldsymbol{\tau} \|, \tag{11}$$

where $\mathbf{q}_h \in \mathbb{R}^n$ is the human joint angle vector and $\Delta\boldsymbol{\tau} \in \mathbb{R}^n$ is the vector of joint torque overloading from (7).

Several constraints were considered in the numerical optimization process, such as upper and lower bounds on the human joint angles $\mathbf{q}_h$; a linear inequality constraint on the CoP, $\mathbf{C}_P \in \mathbb{R}^2$, to keep the postural stability of the human body, constraints on the position of the object; and finally, a constraint for the endpoint manipulability of the human arm (details can be found in [18]). Once an optimal human body configuration was computed, the robot trajectories were calculated online based on the current human hand and its position in the workspace (where the robot end effector was placed) and the optimized one (where the effect of loading is minimized) to facilitate the subject in achieving such ergonomic configurations by following the end-effector movements. The subjects were instructed to adjust their pose following the robot movements and accomplish the task while achieving the optimized configuration.

To assign zero initial and final values to velocity and acceleration and, hence, to achieve smoother trajectories in the transitions between the target robot end-effector points, the desired position and velocity profiles were generated with a fifth-order polynomial. Throughout the trials, the target points and the corresponding trajectories were adaptively modulated based on human displacement in the robot's workspace and changes of the operating hand (see the accompanying video, which can be found as supplemental material for this article in IEEE *Xplore*.). A delay profile of 3 s and a dead-zone displacement of 5 cm for human movements were deliberately introduced in robot trajectory regeneration to avoid agitated and unnecessary robot movements in response to small/fast human displacements.

When a comanipulation task was completed, the operator pushed the robot end effector in the *y* axis (with respect to the robot base frame) to make the robot aware of the task completion. This was accomplished by projecting the estimated external torques to the robot end effector through the pseudoinverse of the Jacobian transpose. As a result, the robot placed the part back and was prepared for the operator's next commands.

Graphical Interface

To make the operator aware of the online estimated body joint overloadings, along with his or her current body configuration, a graphical interface was created. The Robot Operating System 3D visualizer RViz was employed for the display. The joint overloadings were color coded to denote high (red), medium (orange), or low (green) values. The three thresholds were defined based on the data available in ergonomic studies (for example, [32]) and fine-tuned based on the feeling of discomfort among the subjects. Different tools/objects were represented with a different colors/shapes in this graphical interface. Depending on their weight, the external forces and the overloading of joint torques experienced by the human varied.

An example of the information that can be provided in real time to the human is illustrated in Figure 5. Figure 5(a) and (b) indicates the example postures and the joint overloading of a subject without and with a tool (drill) in hand, respectively. In addition, the positions of the measured (red) and the estimated CoP (blue) are illustrated on the ground. In Figure 5(b), three different body configurations are represented, passing from a risky condition, denoted by high values of overloading on the joints, to a safe and comfortable one, in which the physical effort is minimized, as suggested by the lower overloading values. It should be noted that, in

Figure 5(a), the human is operating without any tool and, thus, without the effect of any external forces. Therefore, the overloading on the joints is always low.

Finite-State Machine

The integration of various components described previously into a unified HRC framework was achieved using a global finite-state machine (FSM), depicted in Figure 4. This was due to the requirement for continuous transitions from one state to another in response to the external inputs and to coordinate the data exchange among the three modules. Communication among the different modules of the framework, such as ergonomics, control, and vision, was implemented via UDP messages, while submodules of the vision system utilized YARP protocols (that is, a combination of UDP, Transmission Control Protocol, and so on).

The FSM's initial state is identified by the homing primitive in which the robot end effector is in the center of the workspace waiting for an input from the vision module. When the vision system recognizes that the subject is holding a tool, the object-picking state is triggered, and the robot arm picks the corresponding part, bringing it close to the tool to start the comanipulation stage. In this phase, the stiffness and damping matrices are modulated to avoid deviations from the desired trajectories caused by the part's weight. After receiving the optimization pose from the ergonomics module, the robot moves toward the desired configuration, where the comanipulation can be executed more comfortably. At this stage, three possible actions can be triggered as shown in Figure 4: hand change, human pose change, and external force detection. If the subject moves in the workspace or he or she switches the tool hand, the vision module communicates the relative changes to the control module, and a new path is generated from the trajectory replanning and executed by the move primitive. On the other hand, if external forces are detected on the y axis, the object is returned to its original position, and the robotic arm goes back to the homing configuration.

Experimental Setup

Figure 2 illustrates the experimental setup in our study. As noted previously, we used the KUKA LBR iiwa robotic manipulator equipped with the Pisa/IIT softhand. We chose to use a synergy-driven, underactuated robotic hand because of the mechanical adaptability of the hand to the shapes of the parts, which simplifies grasp planning and control.

All software components were implemented in a C++ environment. The robot was controlled by joint torque, and the torque commands were sent to KUKA using Fast Research Interface (FRI) at 500 Hz. The Cartesian impedance controller in the section "Robot Interaction Controller" was implemented by setting the stiffness and damping gains of the FRI's default joint impedance controller to zeros. This allowed us to directly set the torque references related to the impedance behavior of the robot; in our case, this was the desired stiffness and damping as we targeted quasi-static interactions between humans and the iiwa robot.

The hand was controlled using a custom control board that implements an outer position loop and inner current regulator (that is, impedance controlled) at 1 kHz. The hand control gains were tuned to have a firm grasp of the parts and kept constant during the experiments. The reliability of each module's performance and the communication between modules was important, because a continuous demonstration of the proposed ergonomic and reconfigurable HRC framework for the entire duration of the KUKA Innovation Award (one week, 8 h/day) was a critical measure for success.

Ten healthy subjects (eight males and two females; age, 30.2 ± 3.7 years; weight, 79.6 ± 10.9 kg; and height, 178.4 ± 5.5 cm) participated in the overall experiments. An electric drill/screwdriver (4 kg) and a polisher (3 kg) were placed next to the subjects. Each tool was associated with a part to be manipulated (see also Figure 6). Two components of a robot actuator (outer shell and inner part) were chosen for this purpose. The subjects were asked to pick a tool by choice [Figure 6(a) and (g)], in a random order, perform the manipulation, and push the robot in the y axis [Figure 6(f)] to end the task. While manipulating, the subjects could change hands [Figure 6(c) and (d)] and move in the workspace arbitrarily and repeatedly [Figure 6(e)]. Nevertheless, they were instructed to follow the robot end-effector movements in the sagittal plane (xz) and possibly align the whole-body pose to the one illustrated by the graphical interface [Figure 6(b) and (c)] to achieve ergonomic postures. The current pose and the optimal one were illustrated to the user in black and blue, respectively.

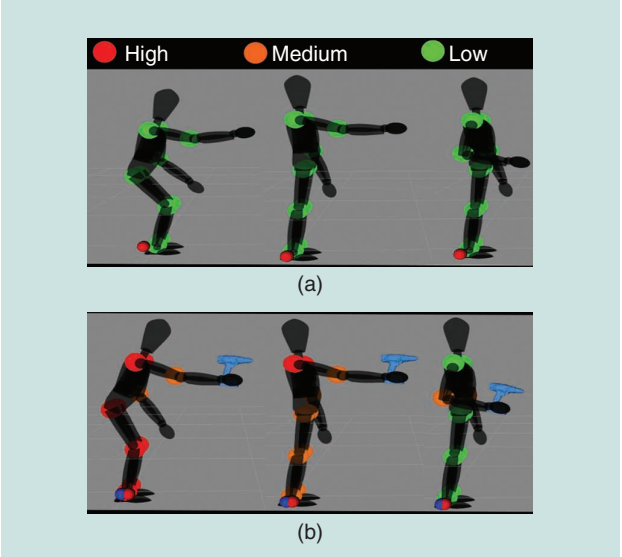

Figure 5. Examples of the information provided by the graphical interface. (a) Example postures without a tool. (b) Example postures with a tool. The levels of joint torque overloading are color coded to denote a high (red), medium (orange), or low (green) value and are illustrated in the main joints of the human body.

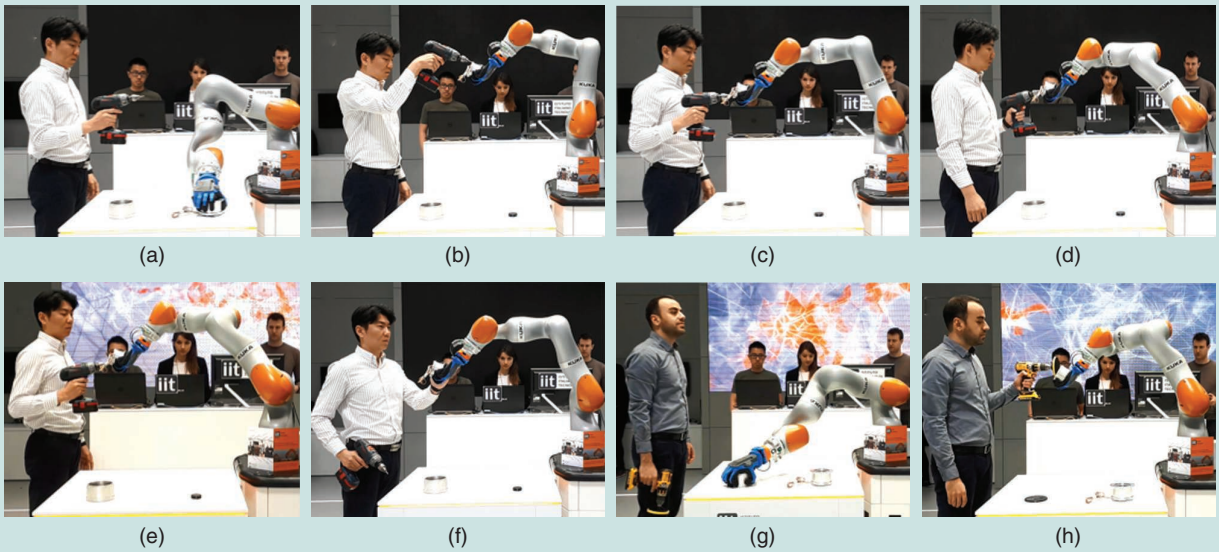

Figure 6. Snapshots of a typical HRC experiment in this study; (a)–(f) represent one test sequence, while (g) and (h) represent another. (a) and (g) The subjects could pick a tool of their choice, and (b) the robot grasped the associated part and gave it to them in a configuration (for the sake of comparison with the ergonomically optimized posture). (c) Next, robot trajectories were optimized online to change the human configuration and so minimize the effect of external load on body joints. (d) and (h) The user could switch hands or (e) move within the workspace, and the robot trajectories were continuously adapted. (f) When the task was accomplished, the user pushed the robot end effector on the *y* axis, to make the robot return the part and prepare for the next commands.

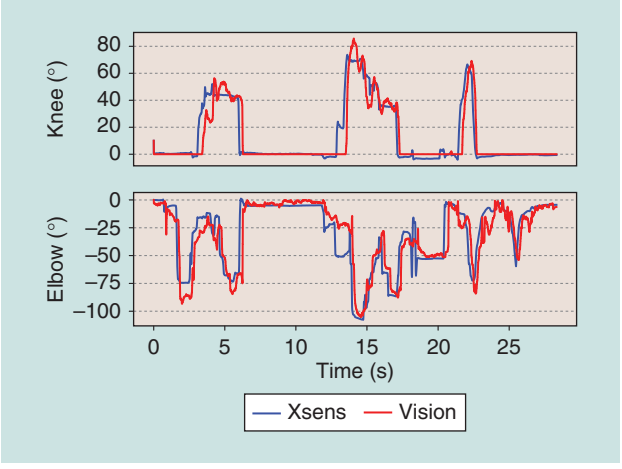

Figure 7. Some typical joint-angle tracking results of the elbow and knee joint provided by the commercial Xsens system and the developed skeleton 3D model (vision module).

Results

Visual Tracking Accuracy

The performance of the vision module was evaluated by estimating the accuracy of the tool and operating hand recognition and the tracking of the human skeleton, i.e., the joint angles and the operator's absolute position in the robot's workspace. The assessment of vision accuracy was crucial for us to understand the performance of the system in a simultaneous tracking of the hand, tool, and body. In particular, the placement of the robotic arm in front of the camera introduced errors to the tracking of human whole-body kinematics because the robotic arm could be confused with the operator's. As mentioned previously, we applied some biometric constraints to resolve such issues.

Regarding the accuracy of the tool (drill versus polisher) and hand recognition (left versus right), we obtained the success rates by comparing the captured screens through the vision module and the actual ones. Ten trials were performed in which 10 subjects were asked to randomly change the tool and the operating hand within each trial. The score for the tool detection accuracy among all subjects was 83.5% ± 0.1% (88.0% ± 0.05% in the right hand and 79.0% ± 0.1% in the left hand).

To evaluate the performance of the vision system in terms of human tracking, we measured the human configuration in terms of joint angles and absolute position in the robot workspace. First, we provide a comparison between the vision system's tracking of human joint angles and the tracking by a commercially available, wearable suit (Xsens Technologies BV, The Netherlands). The root-mean-square error between the joint angles provided by the vision system and the wearable MVN Biomech suit was 6.93° ± 3.86° in the overall 10 joints. The tracked joints were the hips, knees, ankles, shoulders, and elbows on both the left and right.

Typical results of the vision system's tracking of the elbow and knee joint angles (sketched by solid red line) and the wearable suit (solid blue line) are illustrated in Figure 7. The selected joints from the lower body (knee) and upper body (elbow) in this plot are significantly affected by the tool weight in this task. The tracking accuracy of the vision system was adequate experiments calculating the joint torque overloading.

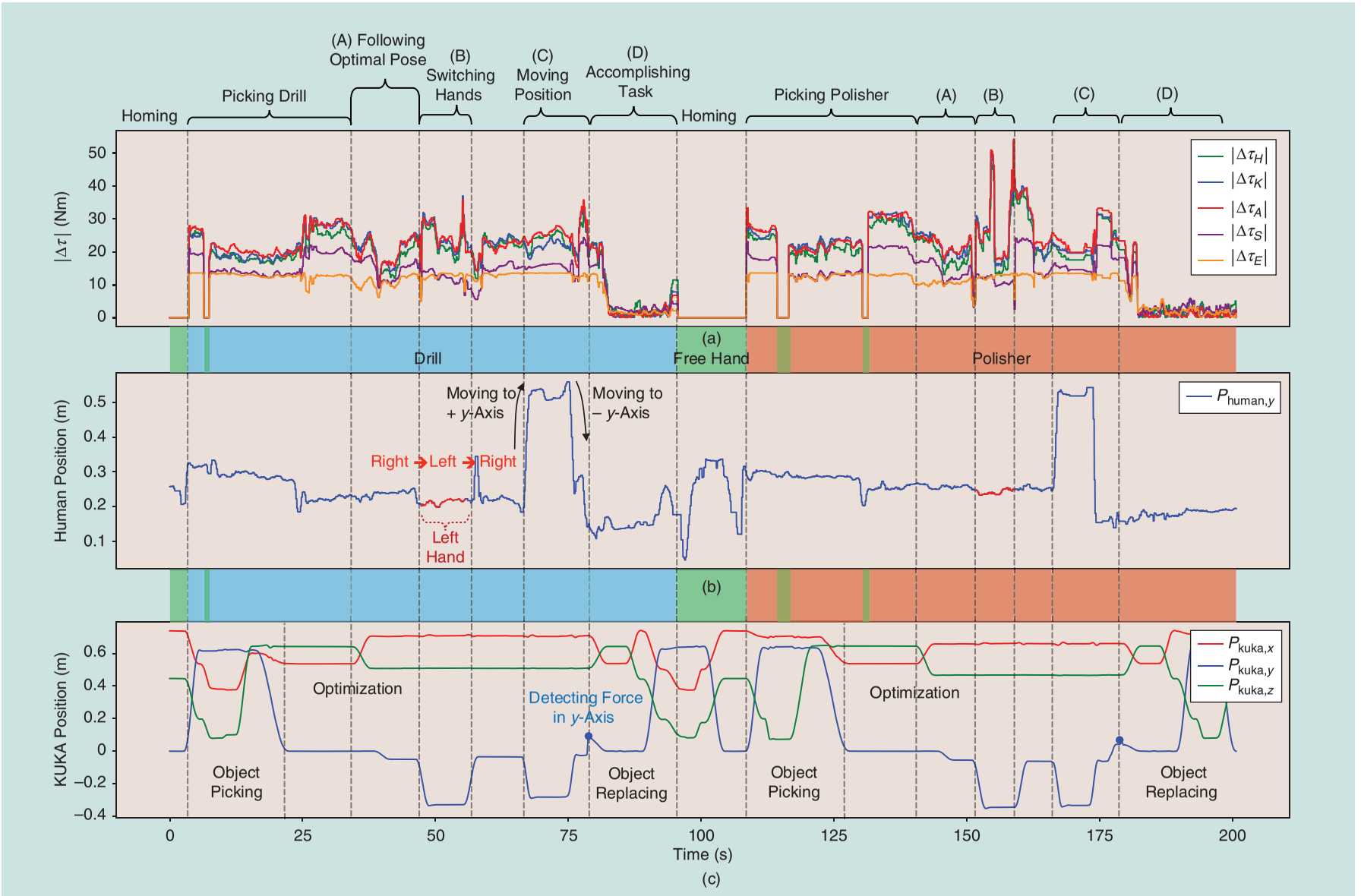

Figure 8. A summary of data collected from subject one (male). (a) The estimated joint torque overloading values by the ergonomics module, (b) the human pose and the tools recognized by the vision module, and (c) the robot Cartesian movements by the control module.

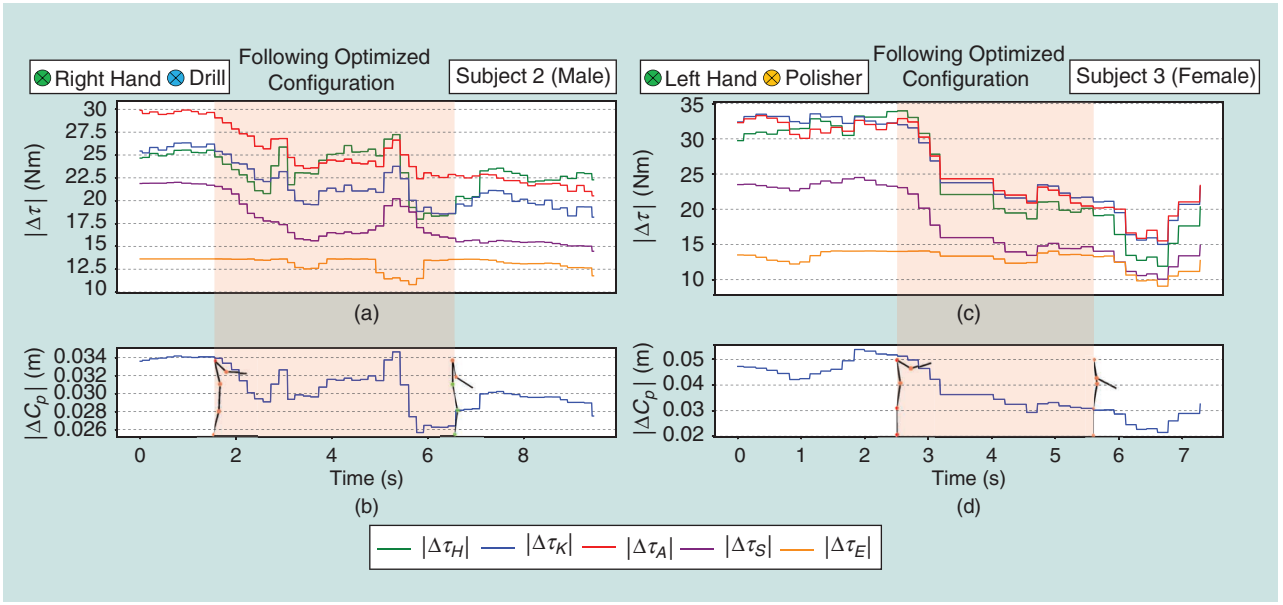

Figure 9. The results for (a) and (b) male subject two and (c) and (d) female subject three for the optimization phase. (a) and (c) The calculated joint torque overloading. (b) and (d) The whole-body CoP displacement caused by the external tool and the subjects' configurations.

Calculating the operator's position error in space required comparing the positions between the measured (via the vision system) position and five predefined positions. To achieve this, the subjects were instructed to relocate their position to different points on the floor (±0.2 m on the x axis and ±0.3 m on the y axis). The position error was 0.06 ± 0.03 m on the x axis and 0.04 ± 0.03 m on the y axis across all 10 subjects.

Human–Robot Comanipulation

Typical results of the comanipulation experiment for a male subject are provided in Figure 8. The variations of joint torque overloading, estimated from the ergonomics module for different tools, are clearly observable in the first row of the plot. The subsequent plots show the human position on the y axis as estimated by the vision module, which was caused by an arbitrary movement in the workspace, and the KUKA LBR iiwa motion in Cartesian space. Between the plots, the tool types provided by the vision module are illustrated in different colors (green, free hand; blue, drill; and red, polisher).

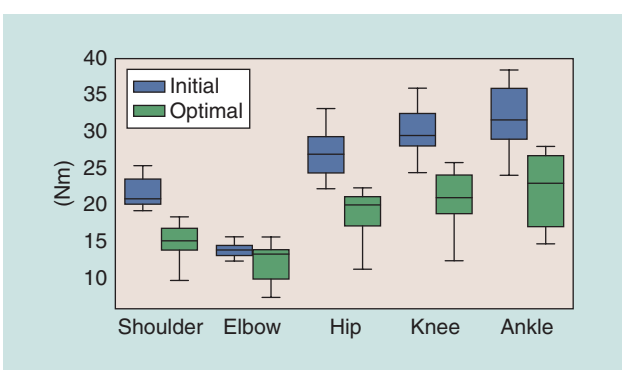

Figure 10. The average (across 10 subjects) joint torque overloading for the initial (blue) and optimal (green) human configuration as guided by the proposed ergonomic HRC framework.

The typical task included two different tool–part combinations (that is, drill–inner shell and polisher–outer shell) (see the section "Experimental Setup"). The subphase (A) refers to the case in which the robot changed its configuration due to the optimization and contributed to the reduction of human joint torque overloading [see also Figure 6(b) and (c)]. In subphase (B), the subject switched hands [Figure 6(d)], and, in subphase (C), the subject moved in the workspace arbitrarily [Figure 6(e)]. In subphase (D), the robot was notified about the task accomplishment [the robot end effector was pushed in the y axis; Figure 6(f)], and the robot placed the object back to a certain position. Between the subphases, the estimated overloading effects were occasionally inaccurate due to the vision error caused by occlusions (for example, the robot covering a part of the human body). The control module did not react in such cases because, between the phases, the robot configuration on the xz-plane was kept fixed for safety reasons.

Subphase (A) is also demonstrated for two other subjects (one male and one female) in Figure 9. Figure 9(a) and (c) represents a deviation of the joint overloading while following the optimized configuration. Figure 9(b) and (d) depicts the distance of the CoP, which was calculated by the effect of the tool mass. Moreover, the initial and final body configurations, also shown by the graphical interface, are illustrated.

All experiments demonstrated a coherent reduction of joint torque overloading in subjects when the robot behavior was optimized (see Figure 10). The average decrement ratio of

the overloading of joint torques for subphase (A) among 10 subjects was 30.24% ± 2.38% (mean ± standard error of mean) as follows: 32.65% ± 16.12% in the hip, 33.50% ± 14.16% in the knee, 32.54% ± 12.44% in the ankle, 37.21% ± 15.23% in the shoulder, and 15.30% ± 17.25% in the elbow. Statistical significance tests were conducted at the 0.05 significance level using the Bonferroni post hoc *t*-test. The optimized configuration showed a significantly lower overloading effect in all joints compared with the initial configurations. The difference values of joint torque overloading in each joint were 8.24 ± 0.97 Nm ($p \leq 0.001$) in the shoulder, 2.13 ± 0.65 Nm ($p \leq 0.001$) in the elbow, 9.29 ± 1.31 Nm ($p \leq 0.001$) in the hip, 10.37 ± 1.26 Nm ($p \leq 0.001$) in the knee, and 10.62 ± 1.18 Nm ($p \leq 0.001$) in the ankle. These results provide solid evidence of the cobot's ability to make online adaptations to human factors and so contribute to better ergonomics.

Conclusions and Future Work

This article presented the development of a unified HRC framework that aims to improve human ergonomics and the reconfigurability of the production/assembly processes in industrial environments. The proposed framework enabled a cobot to simultaneously adapt to user states, such as pose, overloading torques, manipulating hand, positional variations in the workspace, and task condition, by detecting the tools and parts in the workspace.

A human–robot comanipulation task was further considered in this study, with 10 subjects participating in drilling/polishing experiments. The framework was intensely evaluated during the KUKA Innovation Award at Hannover Messe, where we ran 8 h of live daily demonstrations for one entire week. The accuracy of the algorithm in tracking multiple subjects and tools and its robustness to the detection of multiple visitors at the booth (so that robot behavior is adapted to the subject and not a visitor in the crowd) were validated, demonstrating its high potential in realistic industrial environments.

One of the key extensions of this article with respect to our previous approach in [14] was the introduction of an external vision system for real-time tracking of the human's pose and estimation of the human's intention (by recognizing handheld tools). This consideration was intended to improve the cost effectiveness and applicability of the proposed HRC framework in cross-domain industrial scenarios. The accuracy of the human pose tracking using the visual system was evaluated by comparing 10 joints of the human body to the results of a commercial, wearable suit during arbitrary yet extensive whole-body movements. Although the joints of the lower body demonstrated low differences, the upper body joints had slightly higher values: the upper body joints can be covered by human hands or tools during the action, which causes high errors in the vision system's reconstruction step from 2D to 3D (see the section "Human Whole-Body Kinematic Tracking"). Nevertheless, the overall accuracy of the visual tracking system was acceptable for our experiments.

Future work will focus on the introduction of a face recognition component in the vision module so that the SESC parameters of the workers and other subject-specific information can be updated autonomously. This will enable cobots to assist multiple workers, with robot responses optimized to each individual. Next, robot mobility will be added to the framework so that a cobot can follow the subject in the production line and provide assistance. This concept is similar to wearable force-augmenting exoskeletons, with the major difference being that the cobots do not add extra weight to users or affect user comfort.

Acknowledgments

The Human–Robot Interfaces and Physical Interaction Laboratory contributed to the development of human dynamic modeling and optimization, robot interaction control, and feedback interfaces. The iCub Facility and Humanoid Sensing and Perception Laboratory contributed to robotic vision, i.e., object recognition and human kinematic tracking. The work presented here was the winner of the KUKA Innovation competition 2018. Phuong D.H. Nguyen was supported by a Marie Curie Early Stage Researcher Fellowship (H2020-MSCA-ITA, SECURE 642667).

References

[1] A. A. Shikdar and N. M. Sawaqed, "Worker productivity, and occupational health and safety issues in selected industries," *Comput. Ind. Eng.*, vol. 45, no. 4, pp. 563–572, 2003.

[2] M. G. Mehrabi, A. G. Ulsoy, and Y. Koren, "Reconfigurable manufacturing systems and their enabling technologies," *Int. J. Manuf. Technol. Manage.*, vol. 1, no. 1, pp. 114–131, 2000.

[3] A. Ajoudani, A. M. Zanchettin, S. Ivaldi, A. Albu-Schäffer, K. Kosuge, and O. Khatib, "Progress and prospects of the human–robot collaboration," *Auton. Robots*, vol. 42, no. 5, pp. 957–975, 2018.

[4] I. El Makrini, K. Merckaert, D. Lefeber, and B. Vanderborght, "Design of a collaborative architecture for human–robot assembly tasks," in *Proc. 2017 IEEE/RSJ Int. Conf. Intelligent Robots and Systems (IROS)*, 2017, pp. 1624–1629.

[5] B. Matthias and T. Reisinger, "Example application of ISO/TS 15066 to a collaborative assembly scenario," in *Proc. ISR 2016: 47th Int. Symp. Robotics*, 2016, pp. 1–5.

[6] K. Kosuge and N. Kazamura, "Control of a robot handling an object in cooperation with a human," in *Proc. 6th IEEE Int. Workshop Robot and Human Communication*, 1997, pp. 142–147.

[7] D. J. Agravante, A. Cherubini, A. Bussy, P. Gergondet, and A. Kheddar, "Collaborative human-humanoid carrying using vision and haptic sensing," in *Proc. 2014 IEEE Int. Conf. Robotics and Automation*, 2014, pp. 607–612.

[8] L. Peternel, N. Tsagarakis, and A. Ajoudani, "A human–robot comanipulation approach based on human sensorimotor information," *IEEE Trans. Neural Syst. Rehabil. Eng.*, vol. 25, no. 7, pp. 811–822, July 2017.

[9] F. Ficuciello, A. Romano, L. Villani, and B. Siciliano, "Cartesian impedance control of redundant manipulators for human–robot comanipulation," in *Proc. 2014 IEEE/RSJ Int. Conf. Intelligent Robots and Systems*, 2014, pp. 2120–2125.

[10] L. Roveda, "A user-intention based adaptive manual guidance with force-tracking capabilities applied to walk-through programming for

industrial robots," in *Proc. IEEE 2018 15th Int. Conf. Ubiquitous Robots*, 2018, pp. 369–376.
[11] P. Maurice, V. Padois, Y. Measson, and P. Bidaud, "Human-oriented design of collaborative robots," *Int. J. Ind. Ergonom.*, vol. 57, pp. 88–102, Jan. 2017.
[12] L. Fritzsche, "Ergonomics risk assessment with digital human models in car assembly: Simulation versus real life," *Hum. Factors Ergonom. Manuf. Serv. Ind.*, vol. 20, no. 4, pp. 287–299, 2010.
[13] R. W. Proctor and T. Van Zandt, *Human Factors in Simple and Complex Systems*. Boca Raton, FL: CRC Press, 2018.
[14] W. Kim, J. Lee, L. Peternel, N. Tsagarakis, and A. Ajoudani, "Anticipatory robot assistance for the prevention of human static joint overloading in human–robot collaboration," *IEEE Robot. Autom. Lett.*, vol. 3, no. 1, pp. 68–75, 2018.
[15] J. Jovic, A. Escande, K. Ayusawa, E. Yoshida, A. Kheddar, and G. Venture, "Humanoid and human inertia parameter identification using hierarchical optimization," *IEEE Trans. Robot.*, vol. 32, no. 3, pp. 726–735, June 2016.
[16] D. H. P. Nguyen, M. Hoffmann, A. Roncone, U. Pattacini, and G. Metta, "Compact real-time avoidance on a humanoid robot for human–robot interaction," in *Proc. 2018 ACM/IEEE Int. Conf. Human–Robot Interaction*, 2018, pp. 416–424.
[17] G. Pasquale, C. Ciliberto, F. Odone, L. Rosasco, and L. Natale, "Teaching icub to recognize objects using deep convolutional neural networks," *Mach. Learn. Interact. Syst.*, vol. 43, pp. 21–25, 2015.
[18] L. Peternel, W. Kim, J. Babič, and A. Ajoudani, "Towards ergonomic control of human–robot co-manipulation and handover," in *Proc. 2017 IEEE-RAS 17th Int. Conf. Humanoid Robotics*, 2017, pp. 55–60.
[19] Z. Cao, T. Simon, S.-E. Wei, and Y. Sheikh, Realtime multi-person 2D pose estimation using part affinity fields. 2017. [Online]. Available: https://arxiv.org/abs/1611.08050
[20] T.-Y. Lin, et al., "Microsoft coco: Common objects in context," in *European Conference on Computer Vision*, D. Fleet, T. Pajdla, B. Schiele, T. Tuytelaars, Eds. New York: Springer, 2014, pp. 740–755.
[21] A. Krizhevsky, I. Sutskever, and G. E. Hinton, "Imagenet classification with deep convolutional neural networks," in *Proc. Advances Neural Inform. Processing Syst. 25,* 2012, pp. 1097–1105.
[22] G. Metta, P. Fitzpatrick, and L. Natale, "YARP: Yet another robot platform," vol. 3, no. 1, pp. 43–48. [Online]. Available: http://www.intechopen.com/source/pdfs/4161/InTech-Yarp_yet_another_robot_platform.pdf
[23] P. Fitzpatrick, G. Metta, and L. Natale, "Towards long-lived robot genes," *Robot. Auton. Syst.*, vol. 56, no. 1, pp. 29– 45, 2008.
[24] D. A. Winter, "Human balance and posture control during standing and walking," *Gait Posture*, vol. 3, no. 4, pp. 193–214, 1995.
[25] M. B. Popovic, A. Goswami, and H. Herr, "Ground reference points in legged locomotion: Definitions, biological trajectories and control implications," *Int. J. Robot. Res.*, vol. 24, no. 12, pp. 1013–1032, 2005.
[26] P. R. Bélanger, P. Dobrovolny, A. Helmy, and X. Zhang, "Estimation of angular velocity and acceleration from shaft-encoder measurements," *Int. J. Robot. Res.*, vol. 17, no. 11, pp. 1225–1233, 1998.
[27] A. González, M. Hayashibe, V. Bonnet, and P. Fraisse, "Whole body center of mass estimation with portable sensors: Using the statically equivalent serial chain and a kinect," *Sensors*, vol. 14, no. 9, pp. 16,955–16,971, 2014.
[28] J. J. Yang and J. H. Kim, "Static joint torque determination of a human model for standing and seating tasks considering balance," *J. Mech. Robot.*, vol. 2, no. 3, pp. 1–9, 2010.
[29] S. H. Hyon, "Compliant terrain adaptation for biped humanoids without measuring ground surface and contact forces," *IEEE Trans. Robot.*, vol. 25, no. 1, pp. 171–178, Feb. 2009.
[30] A. Albu-Schaffer, C. Ott, U. Frese, and G. Hirzinger, "Cartesian impedance control of redundant robots: Recent results with the DLR-light-weight-arms," in *Proc. IEEE Int. Conf. Robotics and Automation*, 2003, pp. 3704–3709.
[31] A. Dietrich, C. Ott, and A. Albu-Schäffer, "An overview of null space projections for redundant, torque-controlled robots," *Int. J. Robot. Res.*, vol. 34, no. 11, pp. 1385–1400, 2015.
[32] J. C. E. Van Der Burg, J. H. Van Dieën, and H. M. Toussaint, "Lifting an unexpectedly heavy object: The effects on low-back loading and balance loss," *Clin. Biomech.*, vol. 15, no. 7, pp. 469–477, 2000.
[33] Roboception. [Online]. Available: https://roboception.com/product/rc_visard-65-monochrome/

Wansoo Kim, Human–Robot Interfaces and Physical Interaction Laboratory, Istituto Italiano di Tecnologia, Genova, Italy. Email: wan-soo.kim@iit.it.

Marta Lorenzini, Human–Robot Interfaces and Physical Interaction Laboratory, Istituto Italiano di Tecnologia, Genova, Italy. Email: marta.lorenzini@iit.it.

Pietro Balatti, Human–Robot Interfaces and Physical Interaction Laboratory, Istituto Italiano di Tecnologia, Genova, Italy. Email: pietro.balatti@iit.it.

Phuong D.H. Nguyen, iCub Facility, Istituto Italiano di Tecnologia, Genova, Italy. Email: phuong.nguyen@iit.it.

Ugo Pattacini, iCub Facility, Istituto Italiano di Tecnologia, Genova, Italy. Email: ugo.pattacini@iit.it.

Vadim Tikhanoff, iCub Facility, Istituto Italiano di Tecnologia, Genova, Italy. Email: vadim.tikhanoff@iit.it.

Luka Peternel, Human–Robot Interfaces and Physical Interaction Laboratory, Istituto Italiano di Tecnologia, Genova, Italy. Email: luka.peternel@iit.it.

Claudio Fantacci, Humanoid Sensing and Perception Laboratory, Istituto Italiano di Tecnologia, Genova, Italy. Email: claudio.fantacci@iit.it.

Lorenzo Natale, Humanoid Sensing and Perception Laboratory, Istituto Italiano di Tecnologia, Genova, Italy. Email: lorenzo.natale@iit.it.

Giorgio Metta, iCub Facility, Istituto Italiano di Tecnologia, Genova, Italy. Email: giorgio.metta@iit.it.

Arash Ajoudani, Human–Robot Interfaces and Physical Interaction Laboratory, Istituto Italiano di Tecnologia, Genova, Italy. Email: arash.ajoudani@iit.it.